This article was downloaded by:
On: *26 January 2011*
Access details: *Access Details: Free Access*
Publisher *Taylor & Francis*
Informa Ltd Registered in England and Wales Registered Number: 1072954 Registered office: Mortimer House, 37-41 Mortimer Street, London W1T 3JH, UK

Liquid Crystals
Publication details, including instructions for authors and subscription information:
http://www.informaworld.com/smpp/title~content=t713926090

Inversion line in finite samples of ferroelectric liquid crystals with the chevron layer structure

Monique Brunet[a]; Lubor Lejčarek[ab]
[a] Groupe de Dynamique des Phases Condensées (U.R.A. 233), Université de Montpellier II, Montpellier, France [b] Institute of Physics, Na Slovance 2, Prague 8, Czech Republic

To cite this Article Brunet, Monique and Lejčarek, Lubor(1995) 'Inversion line in finite samples of ferroelectric liquid crystals with the chevron layer structure', Liquid Crystals, 19: 1, 1 — 13
To link to this Article: DOI: 10.1080/02678299508036715
URL: http://dx.doi.org/10.1080/02678299508036715

PLEASE SCROLL DOWN FOR ARTICLE

Full terms and conditions of use: http://www.informaworld.com/terms-and-conditions-of-access.pdf

This article may be used for research, teaching and private study purposes. Any substantial or systematic reproduction, re-distribution, re-selling, loan or sub-licensing, systematic supply or distribution in any form to anyone is expressly forbidden.

The publisher does not give any warranty express or implied or make any representation that the contents will be complete or accurate or up to date. The accuracy of any instructions, formulae and drug doses should be independently verified with primary sources. The publisher shall not be liable for any loss, actions, claims, proceedings, demand or costs or damages whatsoever or howsoever caused arising directly or indirectly in connection with or arising out of the use of this material.

LIQUID CRYSTALS, 1995, VOL. 19, NO. 1, 1–13

Inversion line in finite samples of ferroelectric liquid crystals with the chevron layer structure

by MONIQUE BRUNET and LUBOR LEJČEK*†

Groupe de Dynamique des Phases Condensées (U.R.A. 233),
Université de Montpellier II, Case courrier 026, 34095 Montpellier, France
† Institute of Physics, Na Slovance 2, 180 40 Prague 8, Czech Republic

(Received 12 July 1994; in final form 23 December 1994; accepted 3 January 1995)

In finite samples of ferroelectric liquid crystals with parallel smectic layers inclined with respect to the sample surfaces, the chevron structure usually occurs. For the same surface anchoring conditions, the twisted molecular organization may also appear, but in contrast with the bookshelf layer geometry, the twist is confined either to the upper part of the chevron, with the lower part untwisted or vice versa. Therefore two different director configurations with respect to the chevron interface can be recognized. These different configurations can coexist and they can be mediated by the so called inversion line. In this communication, we describe this inversion line within the simplest approximation of the chiral smectic C* elasticity. The self-energy of the inversion line, together with its core energy estimated on the basis of the Peierls–Nabarro model, gives the energetically more favourable solution from two that are possible. Finally the interaction of the inversion line with 2π-twist disinclination (unwinding line) is discussed and used to explain the observed coalescence of parts of these lines in the terms of their mutual interaction.

Downloaded At: 10:03 26 January 2011

1. Introduction

After the first suggestion of tilted layers [1] and of the chevron layer structure [2] in thin samples of ferroelectric liquid crystals (FLC), considerable effort was devoted to proving and explaining the observed optical properties of thin FLC cells on the basis of the chevron structure (see, for example, [3–7]). The application of an external electric field permitted dynamic studies of the director reorientation [8–10] and revealed that in samples with the same anchoring conditions on the surfaces the molecular structure may be twisted only in one part of the sample limited by the internal interface which is the plane of chevron [9, 10]. Moreover the application of a low external electric field can influence the chevron interface in such a way that the chevron profile is either deformed, exhibiting the so called field line defect [11, 12] or has started to be asymmetric with the mountain defect connecting the asymmetric positions of the chevron interface [13]. The mountain defect then connects the chevron parts with the different positions of the chevron interface in the sample.

The molecular twisted structure in one part of the chevron, either above or below the chevron interface, in thin FLC samples without an electric field was also reported in [8, 14, 15]. The optical properties of FLC samples with such a different molecular organization on opposite sides of the chevron interface, i.e. with the twisted structure on one side of the chevron, followed by the uniform structure on the other side, were also studied in [8–17]. The existence of the different molecular orientations with respect to the chevron interface leads to the occurrence of two different states with either the twist in the upper part of the chevron and the uniform arrangement of molecules in its lower part, or the uniform molecular organization in the upper and the twist in the lower part of the chevron, respectively. Therefore there could be either a wall or a line separating these two different states of molecular organization. Such a line, called the inversion line, was in fact observed [15, 16] (see also the photos in [3, 8]). The difference in the light propagation on both sides of the inversion line leads to differently coloured sample parts (called the chevron surface domains in [5, 9]), separated by this inversion line.

In FLC samples with thickness greater than the length $|Z|$ of the helicoidal pitch Z, the helicoidal state appears and is characterized by the system of pairs ($\pm 2\pi$) of twist disclinations, also called unwinding lines, which are situated near the surfaces and which mediate the helicoidal structure in the volume of the sample, with the unwound structure near the sample surfaces [18, 19]. When the anchoring conditions on the sample surfaces lead to the same molecular orientation, favouring a uniform structure

* Author for correspondence.

0267–8292/95 $10·00 © 1995 Taylor & Francis Ltd.

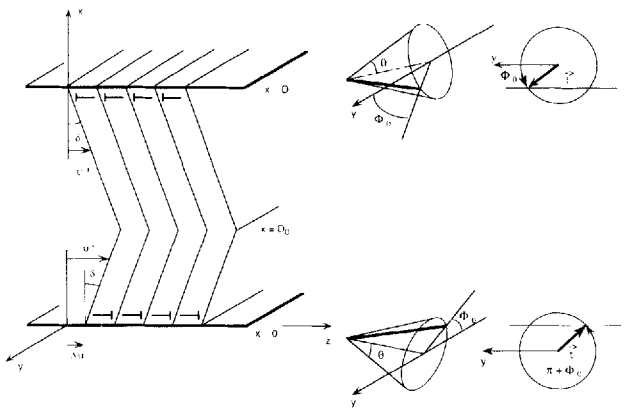

Figure 1. Coordinate system and the liquid crystalline sample. The x axis is perpendicular to the sample surfaces situated at $x = 0$ and $x = D$ and the y axis is parallel to the smectic layers. The smectic layers are inclined at the angle δ from the normal to the sample surfaces. Displacements u^+ and u^- describe the shift of the layers from the reference bookshelf layer structure. The chevron interface is at $x = D_0$. Smectic C* molecules are represented by nails [21] the points of which are turned toward the observer. In this scheme, only the molecules near the upper and lower sample surfaces are shown and also their positions on the surface of the cone with the angle θ which is the tilt angle of molecules with respect to the layer normal. The position of molecules on the surface of the cone is defined by the angle Φ between the molecular projection into the smectic layer (**t** vector) and the y axis. The molecules on the upper sample surface are rotated by the angle Φ_0 from the y axis and molecules on the lower sample surface by the angle $\pi + \Phi_0$.

in thinner samples (so called parallel anchoring conditions), the pairs of disclination lines are superimposed [20]. For symmetric anchoring conditions the relative orientation of molecules at the upper and lower sample surface differs by the angle π, which is the azimuthal angle on the cone describing the possible molecular orientations within the smectic C* layer (see figure 1). Then there is a relative shift on disclination positions near the upper sample surface, with respect to the positions of disclinations near the lower sample surface, of about $|Z|/2$.

Recently both types of systems of disclinations (unwinding lines) were discussed from the more general point of view [20]. In the thicker samples with the chevron structure, where the helicoidal molecular organization is present, the shifted disclination pairs are observed in one part of the chevron and in the other part of the chevron there are superimposed disclination pairs. Such disclination configuration also reveal that within the chevron interface the molecules are nearly parallel as proposed in [5, 6]. Therefore the molecular orientation on one side of the chevron is nearly parallel to the orientation at one sample surface and is rotated by some angle, not necessarily equal to π, with respect to the molecular orientation at the other sample surface.

In the present communication, a simplified model of the molecular orientation near the inversion line will be proposed. The model of the inversion line with given continuous transition between the twisted and uniform states in the upper and lower parts of chevron separated by the chevron interface, with the exception of a line singularity associated with the inversion line. The simplifications and approximations used in this communication are based on the results of chevron models summarized in the next section. The elastic self-energy of the different types of the inversion line will also be calculated, with the core energy estimated on the basis of the Peierls–Nabarro model. Then the interaction between the inversion and unwinding line is discussed.

2. Possible solutions describing the inversion line

Based upon observations of the chevron layer structure in FLC samples, models describing the chevron layer deformation, based on the chiral smectic C* or smectic A elasticity, were proposed [22–27]. The first estimation of the chevron interface thickness based on the molecular orientation elasticity of the nematic type, combined with the compressibility of layers [2], gave the interface thickness ζ about 10 nm and the interface energy $\gamma \sim 10^{-2}$ erg cm^{-2}. The soliton model of the chevron [22] offered similar values for ζ and γ. The chevron interface plays the role of a barrier which does not permit the propagation of orientational deformations of molecules, as, for example, their twist deformation, from one part of chevron to the other. This behaviour was demonstrated both in observations [8, 14–16], and also it follows from the results [27] suggested the existence of the homogeneous and twisted states localized in half parts of the sample separated by the chevron interface.

In order to obtain a simplified description of the inversion line we will use the following approximate model of the chevron: (i) The smectic C* layers in the sample of finite thickness D are inclined from the upper and lower surfaces by the angles δ and $-\delta$, respectively. If the chevron interface is situated at $x = D_0 \neq D/2$, the smectic C* layers are displaced (relatively to the reference state without chevron, where the smectic layers are perpendicular to the sample surfaces), by displacements u^+ and u^- in the upper and lower parts of the chevron (see figure 1). The displacements u^+ and u^- are oriented in the z axis direction and can be expressed as

$$u^+(x) = (D - x)\tan\delta \qquad \text{for} \quad x \in (D_0, D), \quad (1\,a)$$

and

$$u^-(x) = (x + D - 2D_0)\tan\delta \quad \text{for} \quad x \in (0, D_0), \quad (1\,b)$$

Both the molecular tilt angle θ and the layer thickness

Downloaded At: 10:03 26 January 2011

Downloaded At: 10:03 26 January 2011

b will be constant in the upper and lower part of the chevron. The molecular orientation in the layers will be characterized by the **t** vector, which is the orientation of the molecular projection onto the smectic layers. Let the **t** vector make and angle Φ with the y axis. Then the **t** vector can be expressed as $\mathbf{t} = (-\sin\Phi, \cos\Phi)$ in the (x, y) plane, where the x axis is perpendicular to the sample surfaces (see figure 1). To simplify the problem we will study the **t** vector orientation in the reference state and finally transform the reference state by the displacements (1) to the chevron layer structure. Our simplification is therefore valid for small layer tilt angles δ.

The anchoring energies W^+ and W^- on the upper and lower samples surfaces, respectively were proposed in [9] and can be rewritten in the form

$$W^+ = W_M(\sin\Phi_b^+ - \sin\Phi_o)^2, \tag{2a}$$

and

$$W^- = W_M(\sin\Phi_b^- + \sin\Phi_o)^2 \tag{2b}$$

where $W_M = \gamma_1 \sin^2\theta\cos^2\delta$ [9], with γ_1 characterizing the bonding of the molecules to the surfaces. The angles Φ_b^+ and Φ_b^- are the boundary conditions on the upper and lower sample surfaces, respectively, and Φ_o fulfils the relation

$$\sin\Phi_0 = \frac{\tan\delta}{\tan\theta}, \tag{3}$$

for which the director is in the (y, z) plane.

In expressions (2), the polar part of the anchoring energy was neglected. Equation (2a) has minima for $\Phi_b^+ = \Phi_o$, $\pi - \Phi_o$ and $\Phi_b^- = -\Phi_o$, $\pi + \Phi_o$.

(ii) The chevron interface situated at $x = D_o$ (see figure 1) will be taken as a barrier which separates the upper and lower parts of the chevron. We will suppose that the **t** vector orientations Φ^+ and Φ^- in the upper and lower parts of the chevron can be studied independently. Chevron surface anchoring energy W_c can be expressed by analogy with [9] as

$$W_c = \gamma(1 - \cos\chi), \tag{4}$$

where γ is the energy per cm^2 characterizing mainly the layer deformation energy of the chevron interface and the geometric factor $(1 - \cos\chi)$ derived in [9] in the form

$$\begin{aligned} 1 - \cos\chi = {} & 1 - \cos^2\theta\cos 2\delta \\ & - \sin\theta\cos\theta\sin 2\delta\,(\sin\Phi_c^+ - \sin\Phi_c^-) \\ & - \sin^2\theta\cos 2\delta\sin\Phi_c^+\sin\Phi_c^- \\ & - \sin^2\theta\cos\Phi_c^+\cos\Phi_c^-, \end{aligned} \tag{5}$$

where Φ_c^+ and Φ_c^- are the **t** vector orientations on the upper and lower parts of the chevron interface, respectively. In reality there is a coupling between Φ^+ and Φ^- through the **t** vector orientations Φ_c^+ and Φ_c^- on the upper and lower parts of the chevron. This coupling will be discussed later. The values of Φ_c^+ and Φ_c^- corresponding to minima of equation (4), are either $\Phi_c^+ = \Phi_o$ and $\Phi_c^- = -\Phi_o$, or $\Phi_c^+ = \pi - \Phi_o$ and $\Phi_c^- = \pi + \Phi_o$.

(iii) The influence of the FLC spontaneous polarization P_s on the **t** vector distribution will not be taken into account. Therefore our model can be applied only to FLC materials with low values of P_s where it can be assumed that the distribution of charges $\rho(x, z) \sim -\operatorname{div}\mathbf{P}(x, z)$ due to the spatial distribution of the polarization $\mathbf{P}(x, z) = P_s(\cos\Phi, \sin\Phi)$ is either screened by the presence of free charges in the material or can be neglected.

Under the assumptions (i) and (ii), we will treat the upper and lower parts of the chevron independently. The bulk elastic free energy ρf can be then expressed in both parts of the chevron in the form given in [28] for the elastic constants $B_1 = B_2$ and which depends only on derivatives of Φ and not on layer deformations:

$$\rho f = \frac{B_1}{2}\left(\frac{\partial\Phi}{\partial x}\right)^2 + \frac{B_3}{2}\left(\frac{\partial\Phi}{\partial z} - q\right)^2, \tag{6}$$

where B_1 and B_3 are the smectic C* elastic constants and $q = 2\pi/Z$. So in our approximation we use the following expression for the free elastic energy of the sample per unit length in the y direction:

$$\begin{aligned} F = {} & \int_{-R}^{R} dz \int_{o}^{D_o} dx[\rho f]_{\Phi=\Phi^-} + \int_{-R}^{R} dz \int_{D_o}^{D} dx[\rho f]_{\Phi=\Phi^+} \\ & + \int_{-R}^{R} dz[W^+ + W^- + W_c], \end{aligned} \tag{7}$$

where R is the sample dimension in the z direction. The equilibrium equation describing the **t** vector orientations in the upper and lower parts of the chevron and which follows from (7) can be written as

$$B_1\frac{\partial^2\Phi}{\partial x^2} + B_3\frac{\partial^2\Phi}{\partial z^2} = 0, \tag{8}$$

for both $\Phi = \Phi^+$ and $\Phi = \Phi^-$.

In our approximation, the solutions to (8) can be written by analogy with the solutions describing surface π-twist disclinations [29]. Let the line singularity connecting the twisted and homogeneous director orientations in the upper part of the chevron be situated at the point $x = D_o$, $z = 0$. Then the solution $\Phi^+(x, z)$ can be proposed in the form

$$\begin{aligned} \Phi^+(x, z) = {} & \frac{\Delta\Phi^+}{\pi}\arctan\left[\tanh\left(\frac{\pi z}{2\alpha(D - D_o)}\right)\right. \\ & \left.\times\operatorname{cotan}\left(\frac{\pi(x - D_o)}{2(D - D_o)}\right)\right] \\ & + \frac{\Delta\Phi^+}{2}\frac{x - D}{D - D_o} + \Phi_b^+, \end{aligned} \tag{9a}$$

where $\alpha = (B_3/B_1)^{1/2}$. The solution $\Phi^+(x,z)$ satisfies the equilibrium equation (8) and has the value $\Phi^+(x=D,z)=\Phi_b^+$ on the upper sample surface. On the upper part of the chevron interface it is

$$\Phi^+(x=D_o,z)=\frac{\Delta\Phi^+}{2}\left(\frac{z}{|z|}-1\right)+\Phi_b^+=\Phi_c^+,$$

which means that the angle Φ_c^+ of the **t** vector orientation on the chevron interface has a discontinuous change at $z=0$.

As for the behaviour of the solution $\Phi^+(x,z)$ far from the singularity, it is

$$\Phi^+(x,z\to+\infty)=\Phi_b^+ \quad \text{(uniform director distribution)},$$

and

$$\Phi^+(x,z\to-\infty)=\Phi_b^+ + \Delta\Phi^+\frac{x-D}{D-D_o}$$

(twisted director distribution),

The value $\Delta\Phi^+=\Phi_b^+-\Phi_c^+$ determined in the twisted domain of the upper part of the chevron where $\Phi_b^+\neq\Phi_c^+$ is connected with the Frank vector $\Omega^+=(0,0,\Omega^+)$ of this surface twist disclination as $\Omega^+=-\Delta\Phi^+$.

Analogously, the solution at the lower part of the chevron and situated at $x=D_o$, $z=0$ can be written in the form

$$\Phi^-(x,z)=\frac{\Delta\Phi^-}{\pi}\arctan\left[\tanh\left(\frac{\pi z}{2\alpha D_o}\right)\tan\left(\frac{\pi x}{2D_o}\right)\right]+\frac{\Delta\Phi^-}{2}\frac{x}{D_o}+\Phi_b^-, \qquad (9b)$$

which has the value $\Phi^-(x=0,z)=\Phi_b^-$ at the lower sample surface. On the lower part of chevron interface we find

$$\Phi^-(x=D_o,z)=\frac{\Delta\Phi^-}{2}\left(\frac{z}{|z|}+1\right)+\Phi_b^-=\Phi_c^-,$$

with the discontinuous change of Φ_c^- at $z=0$. Far from the singularity it is

$$\Phi^-(x,z\to+\infty)=\Phi_b^-+\Delta\Phi^-\frac{x}{D_0}$$

which describes the twist in the **t** vector orientation and

$$\Phi^-(x,z\to-\infty)=\Phi_b^-$$

gives the uniform **t** vector distribution. The value $\Delta\Phi^-=\Phi_c^--\Phi_b^-$, $\Phi_c^-\neq\Phi_b^-$, determines the value Ω of the Frank vector $\Omega^-=(0,0,\Omega^-)$ and $\Omega^-=\Delta\Phi^-$.

It should be noted, however, that the solutions are situated at the same point $x=D_o$, $z=0$. In reality these solutions are separated by the chevron interface which acts here as the barrier preventing the propagation of the twist as assumed in (ii). In our model the chevron interface thickness is neglected, as its thickness of about 10 nm is comparable with the core dimensions of line singularities. The argument for situating both solutions $\Phi^+(x,z)$ and $\Phi^-(x,z)$ at the same point, for example, $z=0$, follows from the inspection of the chevron interface energy given by (4) and (5): if we suppose for the moment that the surface disclination on the upper part of the chevron interface is displaced with respect to the surface disclination on the lower part of interface, e.g. by a distance Δz in the z direction, on the part of the chevron interface of length Δz, the boundary values Φ_c^+ and Φ_c^- are combined in such a way that the elevation angle χ [9] between the molecular orientation on the upper and lower sides of the chevron interface is non-zero, which does not correspond to the minimum of W_c. The minimum of W_c is therefore obtained for $\Delta z=0$.

A similar argument can be used when only one twist disclination is necessary to describe the connection between the twisted and uniform domains in one part of the chevron, leaving the other part with the uniform **t** vector arrangement. Such a disclination can then be situated either on the sample surface or on one of the chevron interfaces. Whether the sample surface or chevron interface will be preferred by the surface disclination depends on a comparison of the anchoring energies (2) and (4).

In real observations [15, 16], such a disclination was found to be localized at the sample surface. If we situate this disclination on the upper sample surface, for example, we can adapt the solution (9*b*) in the following way:

$$\Phi^+(x,z)=\frac{\Delta\Phi^+}{\pi}\arctan\left[\tanh\left(\frac{\pi z}{2\alpha(D-D_o)}\right)\times\tan\left(\frac{\pi(x-D_o)}{2(D-D_o)}\right)\right]+\frac{\Delta\Phi^+}{2}\frac{(x-D_o)}{(D-D_o)}+\Phi_c^+, \qquad (9c)$$

and

$$\Phi^-(x,z)=\Phi_c^-=\Phi_b^-. \qquad (9d)$$

As expected the solution (9*c*) gives at $x=D$ the change of the boundary **t** vector orientation Φ_b^+ at $z=0$:

$$\Phi^+(x=D,z)=\frac{\Delta\Phi^+}{2}\left(\frac{z}{|z|}+1\right)+\Phi_c^+=\Phi_b^+,$$

with $\Delta\Phi^+=\Phi_b^+-\Phi_c^+$ for $\Phi_b^+\neq\Phi_c^+$. On the upper chevron interface it is $\Phi^+(x=D_o,z)=\Phi_c^+$. Far from the singularity, we again find either the twisted state

$$\Phi^+(x,z\to+\infty)=\Phi_c^++\Delta\Phi^+\frac{(x-D_o)}{(D-D_o)},$$

or the uniform state $\Phi^+(x,z\to-\infty)=\Phi_c^+$.

Downloaded At: 10:03 26 January 2011

There could also be another possibility when disclinations are situated on the upper and lower sample surface instead of on the upper and lower chevron interface. Such surface disclinations were described in [29]. In this case, however, there is not the necessity that both surface disclinations are situated at the same positions along the z axis. This situation can be simply distinguished by optical observations.

3. The elastic self-energy of the inversion line

The elastic energies of the upper and lower parts of the chevron with twist disclinations modelling the inversion line are defined by the formulae

$$E_s^+ = \int_{-R}^{R} dz \int_{D_o}^{D} dx[\rho f]_{\Phi=\Phi^+}$$

and

$$E_s^- = \int_{-R}^{R} dz \int_{o}^{D_o} dx[\rho f]_{\Phi=\Phi^-},$$

with the solutions Φ^+ and Φ^- expressed by (9 *a*) and (9 *b*). Finally we obtain

$$E_s^+ = B_3 q^2 (D - D_o) R - \frac{B_3 q}{2} \Delta\Phi^+ (D - D_o) + I^+, \quad (10\,a)$$

with

$$I^+ = \frac{B_1 R (\Delta\Phi^+)^2}{4(D - D_o)} + \frac{(\Delta\Phi^+)^2 \sqrt{(B_1 B_3)}}{2\pi} \ln \left| \frac{\sinh \dfrac{\pi R}{2\alpha(D - D_o)}}{\sinh \dfrac{\pi r_o}{2\alpha(D - D_o)}} \right|,$$

where r_o is the core radius of the surface disclination. The first term in (10 *a*) is the energy of the unwound sample; the second term describes the influence of the helicity on the molecular twist. The term I^+ contains both the energy of the twisted deformation of the molecular order and the disclination elastic self-energy. Similarly

$$E_s^- = B_3 q^2 D_o R - \frac{B_3 q}{2} \Delta\Phi^- D_o + I^-, \quad (10\,b)$$

with

$$I^- = \frac{B_1 R (\Delta\Phi^-)^2}{4 D_o} + \frac{(\Delta\Phi^+)^2 \sqrt{(B_1 B_3)}}{2\pi} \ln \left| \frac{\sinh \dfrac{\pi R}{2\alpha D_o}}{\sinh \dfrac{\pi r_o}{2\alpha D_o}} \right|,$$

The total self-energy E_s of the inversion line in the sample with the chevron layer structure can be summarized as

$$E_s = E_s^+ + E_s^- + \int_{-R}^{R} dz[W^+ + W^- + W_c], \quad (11\,a)$$

which for anchoring energies independent of the z variable finally gives

$$E_s = E_s^+ + E_s^- + 2R[W^+ + W^- + W_c]. \quad (11\,b)$$

Note that there is not an elastic interaction between the upper and lower disclination because they are separated by the chevron interface which is, according to our assumption (ii) a strong barrier to the propagation of the twist deformation of the molecular orientation.

4. Discussion of possible types of inversion lines

In previous sections, the solutions describing the inversion lines were given in the general form. In this part, the configurations of possible inversion lines will be discussed using the boundary conditions on the sample surface corresponding to the minima of surface and chevron interface energies (2) and (4) schematically represented in figure 2.

Figure 2 (*a*) shows the situation when the twists in molecular orientations in the upper and lower parts of the chevron are oriented in the same sense. On the sample surfaces, we choose $\Phi_b^+ = \Phi_o$, i.e. surface anchoring (2) is strong and $\Phi_b^- = \pi + \Phi_o$. Then the **t** vector orientations on the chevron interface can be either $\Phi_c^+ = \pi - \Phi_o$ and $\Phi_c^- = \pi + \Phi_o$ on the left side of the inversion line or $\Phi_c^+ = \Phi_o$ and $\Phi_c^- = -\Phi_o$ on the right side of the inversion line. The corresponding strengths of the upper and lower disclinations comprising the inversion line are therefore $\Delta\Phi^+ = \Phi_b^+ - \Phi_c^+ = -\pi + 2\Phi_o$ $(z < 0)$ and $\Delta\Phi^- = \Phi_b^- - \Phi_c^- = -\pi - 2\Phi_o$ $(z > 0)$. The twists in the upper and lower parts of the chevron turn in the same sense, but, due to the boundary conditions Φ_b^+ and Φ_b^-, the

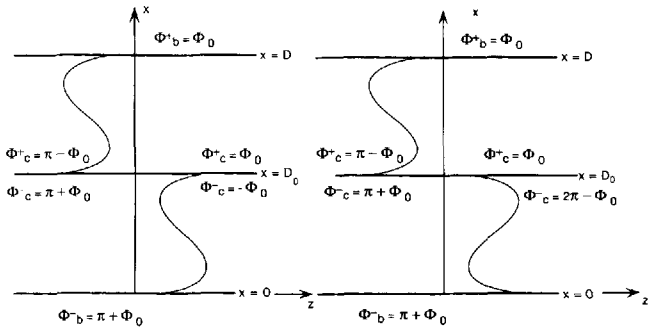

Figure 2. Schematic drawing of the molecular twists and uniform structures in the upper and lower parts of the chevron. The **t** vector orientations on the upper and lower sample surfaces were chosen as $\Phi_b^+ = \Phi_o$, and $\Phi_b^- = \pi + \Phi_o$, respectively. The orientations Φ_c^+ and Φ_c^- on the upper and lower chevron interfaces have the discontinuity at $x = D_o$, $z = 0$ where the inversion line is situated. (*a*) The molecular twists in the upper and lower parts of the chevron turn in the same direction. (*b*) The molecular twists turn in the opposite directions.

Downloaded At: 10:03 26 January 2011

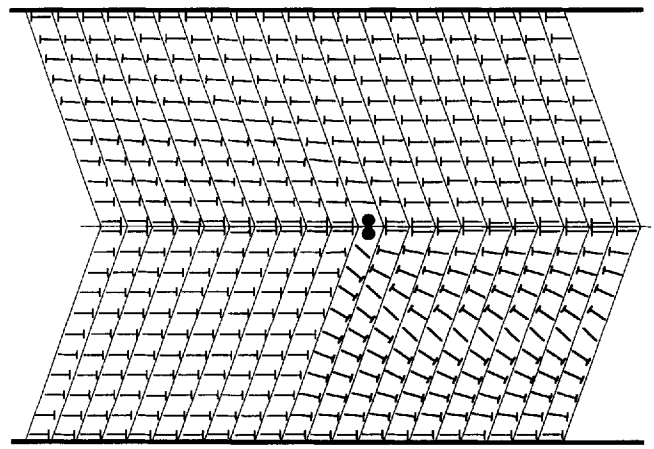

(*a*)

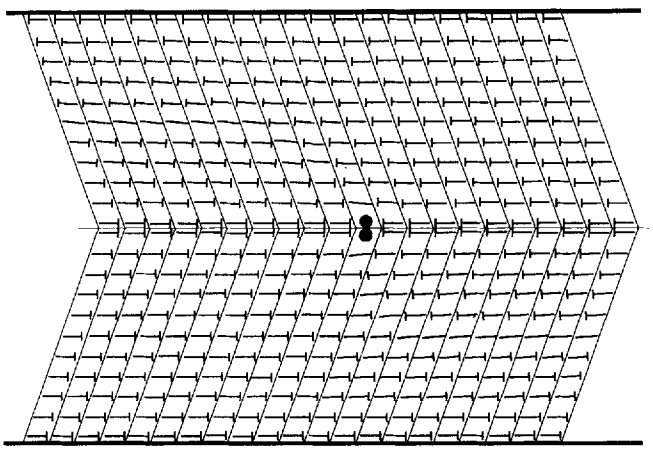

(*b*)

Figure 3. Director distribution near the inversion lines in the nail representation [21] based on the formulae (9 *a*) and (9 *b*) for the model FLC material with $\theta = 22°$, $\delta = 18°$, and $\Phi_o = 53°$ taken from [8], $\alpha = 0{\cdot}32$ and $D_o = D/2$. The layer thickness shown in this figure corresponds to the distance $0{\cdot}1\,D_o$. (*a*) Asymmetric inversion line; (*b*) Symmetric inversion line.

molecules in the lower part of chevron should rotate over the greater part of the cone, and so $|\Delta\Phi^+| < |\Delta\Phi^-|$. Let us call this type of inversion line the asymmetric inversion line (see figure 3 (*a*)).

In figure 2 (*b*) the other possible configuration of the minimum boundary conditions on the chevron interface is shown with the same Φ_b^+ and Φ_b^- as in figure 2 (*a*). For this type of inversion line we have either $\Phi_c^+ = \pi - \Phi_o$ and $\Phi_c^- = \pi + \Phi_o$ for $z < 0$, or $\Phi_c^+ = \Phi_o$ and $\Phi_c^- = 2\pi - \Phi_o$ for $z > 0$ which gives $\Delta\Phi^+ = -\pi + 2\Phi_o$ $(z < 0)$ and $\Delta\Phi^- = \pi - 2\Phi_o$ $(z > 0)$. The molecules turn in the opposite senses in the upper and lower parts of the chevron and so $\Delta\Phi^+ = -\Delta\Phi^-$. This type of inversion line will be called the symmetric inversion line (see figure 3 (*b*)).

Inspection of the total self-energy E_s of the inversion line given by equation (11 *b*) shows that there is a minimum of E_s for $D_o = D/2$ and $|\Delta\Phi^+| = |\Delta\Phi^-|$ which corresponds to the symmetric type of inversion line. In this case, the chevron profile is also symmetric with respect to the chevron interface situated at $x = D/2$, as seen from equations (1) giving $u^+(x = D) = u^-(x = 0)$ with $u^+(x = D/2) = u^-(x = D/2)$. Nevertheless, the chevron interface can be situated in the sample at $x \neq D/2$ as indicated, for example in [8–10, 13]. Therefore we will discuss first the chevron profile shown in figure 1 and then the consequence of such a chevron geometry for the existence of inversion lines.

If we imagine the displacement of the chevron interface from $x = D/2$ to $x = D_o \neq D/2$, with the smectic layers fixed on the surfaces, the equations (1) show that the layers should be shifted by the displacement $\Delta u = (D - 2D_o)\tan\delta$. This displacement can be realized by creating and passing N_s edge dislocations having the Burgers vector **b** of length equal to the smectic C* layer thickness. The number of edge dislocations N_s is then $N_s = \Delta u/b$. In figure 1, the displacement Δu is shown on the lower sample surface, but this does not mean that the shift occurred there. Edge dislocations are created and glide in the sample volume. After their passing the upper layers are reconnected with those in the lower part of the chevron situated at a distance Δu with respect to the initial configuration. This coherent reconnection of smectic layers schematically shown in figure 1 is possible only when D_o satisfies the condition $\Delta u = nb/\cos\delta$, where n is a whole number. Such a procedure requires the overcoming of the energy barrier $\Delta W \sim N_s E_d$, where E_d is the dislocation self-energy per unit length in the y direction. Let us take as E_d the dislocation self-energy calculated in [21] for smectic A, i.e. $E_d \sim Kb^2/(2\lambda r_o)$, with $\lambda^2 = K/B_c$, where K and B_c are smectic elastic constants of the layer bend and the layer compression, respectively. If we take $\lambda \sim r_o \sim b$, the $\Delta W \sim K(D - 2D_o)\tan\delta/(2b)$. For $D - 2D_o \sim 0{\cdot}5\,\mu m$, $\delta \sim 18°$, $b \sim 3\,nm$ and $K \sim 10^{-6}$ dyn, the energy barrier $\Delta W \sim 2 \times 10^{-5}$ dyn. In thin samples of the dimensions $R > D$, the elastic energy stored in the molecular twist deformation could be comparable with ΔW (the energy of the twist deformation can be estimated as $W_T \sim B_1(\Delta\Phi^+)^2 R/D$; for $B_1 \sim 10^{-6}$ dyn, $\Phi_o \sim 53°$ [8] and $R \sim 10D$ it is $W_T \sim \Delta W$), but in such a case the uniform **t** vector orientation is preferred in the sample at the expense of anchoring energy increase. Moreover, the creation and glide of dislocations is the dynamically process not considered in our static estimations. In thick samples the twist deformation energy will be lower then ΔW. Therefore when the chevron interface is created, it can be moved only by the influence of an external field which can create a sufficient number of dislocations as discussed in [10, 11, 13]. So if the chevron with the interface at $x = D_o \neq D/2$ and with the same layer

Downloaded At: 10:03 26 January 2011

inclination δ at the upper and lower sample surfaces occurs, it was created during the phase transition smectic A–smectic C*.

If we assume the existence of a chevron with the interface at $x = D_0$, we can further discuss the existence of an asymmetric inversion line in such a geometry. Let us compare the energies E_s^S and E_s^A of the symmetric and asymmetric inversion lines, respectively, for $D_0 \neq D/2$. With the boundary **t** vector orientations shown in figure 2, the surface anchoring energies in the expression (11 *b*) are zero. Supposing further that the sample dimension (or the distance between inversion lines) $R > D$ and $r_0 \ll D$, we can take $\sinh(\pi R/2\alpha(D - D_0))) \sim \exp(\pi R/2\alpha(D - D_0)))/2$ and $\sinh(\pi r_0/(2\alpha(D - D_0))) \sim \pi r_0/(2\alpha(D - D_0))$ and rewrite the self-energy E_s in the form

$$E_s = B_3 q^2 DR - \frac{B_3 q}{2}[\Delta\Phi^+(D - D_0) + \Delta\Phi^- D_0] + \frac{B_1 R}{2}\left[\frac{(\Delta\Phi^+)^2}{D - D_0} + \frac{(\Delta\Phi^-)^2}{D_0}\right] + \frac{\sqrt{(B_1 B_3)}}{2\pi}\left[(\Delta\Phi^+)^2 \ln\left|\frac{\alpha(D - D_0)}{\pi r_0}\right| + (\Delta\Phi^-)^2 \ln\left|\frac{\alpha D_0}{\pi r_0}\right|\right]. \quad (12)$$

For simplicity, the logarithmic part of E_s can be approximated as $\ln[\alpha D/(2\pi r_0)]$. By designing $E_0 = (\Delta\Phi^+)^2[(B_1 B_3)^{1/2}/(2\pi)] \ln[\alpha D/(2\pi r_0)]$, the self-energy E_s^S can be estimated as

$$E_s^S = B_3 q^2 DR + \frac{B_3 q|\Delta\Phi^+|}{2}(D - 2D_0) + \frac{B_1 R(\Delta\Phi^+)^2}{2}\left[\frac{1}{D - D_0} + \frac{1}{D_0}\right] + 2E_0,$$

and E_s^A as

$$E_s^A = B_3 q^2 DR + \frac{B_3 q|\Delta\Phi^+|}{2}(D - D_0 + \beta D_0) + \frac{B_1 R(\Delta\Phi^+)^2}{2}\left[\frac{1}{D - D_0} + \frac{\beta^2}{D_0}\right] + (1 + \beta^2)E_0,$$

where $\beta = |\Delta\Phi^-/\Delta\Phi^+| > 1$. For the configurations shown in figure 2, the asymmetric configuration is possible only for $q < 0$. Taking $q = -|q|$, the inequality $E_s^A < E_s^S$ leads to the relation

$$D_0 \geq |Z|(\beta - 1)\left[\frac{R}{D_0}\frac{1}{\alpha^2}\frac{|\Delta\Phi^+|}{2\pi} + \frac{E_0}{\pi|\Delta\Phi^+|B_3}\right], \quad (13)$$

which for $R > D_0$, $\delta \sim 18°$, $\Phi_0 \sim 35°$ and $\alpha \sim 0{\cdot}32$ (in [28] the estimation of α was given as $\alpha \sim 0{\cdot}255$) definitely gives $D_0 \gg |Z|$. Therefore, within our approximation, the asymmetric inversion line is not favoured in thin unwound samples the thickness of which is smaller than $|Z|$ [20]. The reason for such a behaviour is connected with the fact that on the one hand the energy of twist deformation $RB_1(\Delta\Phi^-)^2/2D_0$ decreases for $D_0 > D/2$, but on the other hand the energy $RB_1(\Delta\Phi^+)^2/2(D - D_0)$ increases with $D - D_0 < D/2$. The helicity of the liquid crystal could favour the **t** vector rotation $\Delta\Phi^-$ over the greater segment of the cone, but the energy of this interaction is not sufficient when $\alpha < 1$, as can be seen from the inequality (13). Nevertheless, due to the approximation (ii), the interaction energy between surface disclinations representing the inversion line is neglected in the inequality (13).

Up to now we have assumed the chevron interface as one plane situated either at $x = D/2$ or at $x = D_0 \neq D/2$. However, the observation of the mountain defect [13] indicates that during the phase transition, the position of the chevron interface can vary within the sample thickness. Let us suppose that the position of the chevron interface for $z < 0$ is situated at $x = D_1$ and for $z > 0$ at $x = D_2$, as schematically shown in figure 4. Then for the chevron interface geometry of figure 4, we can make similar energy estimations for symmetric and asymmetric inversion lines. In this case, however, we will approximate the inversion line by the inversion wall separating the twisted and uniform structures (or the symmetric and parallel boundary conditions) at $z = 0$. Such an estimation leads again to the relation $D_2 \gg |Z|$. These estimations based on the simplified smectic C* elasticity show that asymmetric inversion lines have always greater elastic self-energy than symmetric inversion lines.

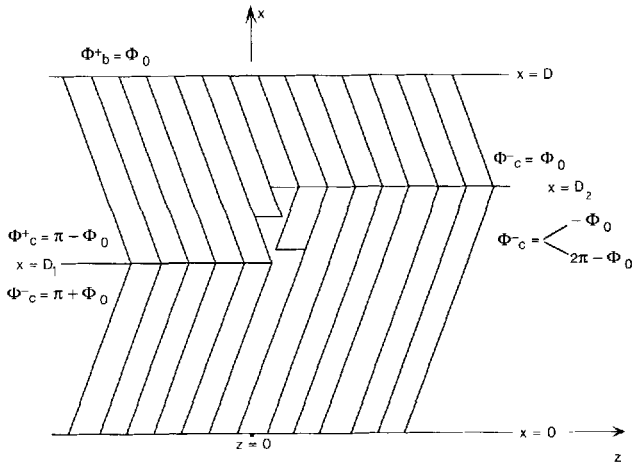

Figure 4. The chevron interfaces situated at $x = D_1$ and $x = D_2$ can be mediated by, for example, the edge dislocation wall, schematically shown at $z = 0$ in the interval $x \in (D_1, D_2)$. Boundary **t** vector orientations are shown at the sample surfaces and on the chevron interfaces. The present chevron interface geometry reminds one of the mountain defect in [13]. (The mountain defect in [13] is oriented in the z direction and this can be modelled by a screw dislocation wall, for example).

Downloaded At: 10:03 26 January 2011

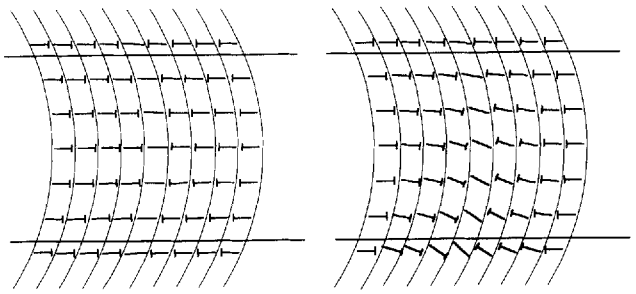

(a) (b)

Figure 5. Schematic surface molecular distributions on the chevron interfaces i^+ and i^- without a singularity on the interfaces i^+ and i^-. (*a*) 2π-disclination core with the smectic A type of the molecular order within the chevron interface. The molecules on the upper and lower parts of the chevron interface rotate in opposite directions. (*b*) No topological defect is necessary when the molecules on the chevron interface rotate in the same sense.

5. Core energy of the inversion line

In the previous parts of this communication, we have assumed the chevron interface to be a barrier which separates the deformations of the orientational molecular order in the upper and lower parts of the chevron. Nevertheless, the expression (4) for the chevron surface anchoring energy, together with equation (5), couples the boundary **t** vector orientations described by Φ_c^+ and Φ_c^- on both surfaces of the chevron interface. Let us suppose now that the inversion line has no singularity in **t** vector orientations at $z = 0$, but that there is a continuous change of Φ_c^+ and Φ_c^- from one side of the inversion line to the other. Therefore Φ_c^+ and Φ_c^- will now depend on the variable z (see figure 5). An example of a model which can determine the functions $\Phi_c^+(z)$ and $\Phi_c^-(z)$ is the Peierls–Nabarro model. The Peierls–Nabarro model, developed for the description of a dislocation core in solid crystals, was adapted to model the surface disclinations in nematics [21, 30] and used for the discussion of the 2π-surface twist disclination in chiral smectic C* liquid crystals in [31]. In the case of the inversion line composed of two disclinations situated on the upper and lower parts of the chevron interface, the core structure will be described by the continuous functions $\Phi_c^+(z)$ and $\Phi_c^-(z)$ which satisfy the coupled non-linear Peierls–Nabarro integro-differential equations:

$$-\frac{\partial W_c}{\partial \Phi_c^+} = \frac{\sqrt{(B_1 B_3)}}{\pi} \int_{-\infty}^{+\infty} \frac{d\Phi_c^+(z')}{dz'} \frac{dz'}{z - z'}, \qquad (14a)$$

and

$$-\frac{\partial W_c}{\partial \Phi_c^-} = \frac{\sqrt{(B_1 B_3)}}{\pi} \int_{-\infty}^{+\infty} \frac{d\Phi_c^-(z')}{dz'} \frac{dz'}{z - z'}, \qquad (14b)$$

where the integrals should be understood as the principal values. Equations (14) express the equilibrium between the torques of molecular twist deformations acting on the upper and lower parts of the chevron interface, where they are balanced by the torques due to the surface anchoring energy [21, 30]. In equation (14), the surface anchoring energy W_c is given by (4).

Comparison of the derivatives of W_c with respect to Φ_c^+ and Φ_c^- in the equations (14) shows that the solutions $\Phi_c^+(z)$ and $\Phi_c^-(z)$ should satisfy the relation

$$\Phi_c^+(z) = -\Phi_c^-(z),$$

which corresponds to the opposite rotations of molecules on the surface of the cone. The inversion line core energy W_{core} is defined as

$$W_{core} = \int_{-\infty}^{+\infty} W_c(\Phi_c^+(z), \Phi_c^-(z))\, dz. \qquad (15)$$

Using the equations (14), it can be shown that the core energy W_{core} does not depend on the explicit forms of W_c, $\Phi_c^+(z)$ and $\Phi_c^-(z)$ (see, for example, [21, 30, 31]) and that it can be expressed in the simple form

$$W = \frac{\sqrt{(B_1 B_3)}}{\pi} [\Phi_c^+(z \to +\infty) - \Phi_c^+(z \to -\infty)]^2. \qquad (16)$$

As W_c depends on the elevation angle χ, we can expect the lower W_{core} for lower values of χ. The lowest possible values of χ can be obtained when molecules rotate over the shortest part of the cone between the values $\chi = 0$ at $\Phi_c^+ = \Phi_c^- = \Phi_o$ and $\chi = 2(\theta - \delta)$ at $\Phi_c^+ = \pi/2$ and $\Phi_c^- = -\pi/2$. This situation corresponds to the boundary conditions shown in figure 2(*b*) for the symmetric inversion line that gives

$$\Phi_c^+(z \to +\infty) - \Phi_c^+(z \to -\infty) = \Delta\Phi^+.$$

If we suppose that the solution of (14) exists for the symmetric inversion line, then its core energy is

$$W_{core} = \pi\sqrt{(B_1 B_3)} \left(\frac{\Delta\Phi^+}{\pi}\right)^2. \qquad (17)$$

The asymmetric inversion line core cannot be described in our approximation of the Peierls–Nabarro model because the **t** vector turns in the same direction on the surface of the cone. Therefore we cannot estimate the core energy of the asymmetric inversion line within the frame of the Peierls–Nabarro model, but we can expect that the core energy is lower for the symmetric inversion line compared with the asymmetric one. For the asymmetric inversion line, the lowest possible values of χ are situated between $\chi = 0$ ($\Phi_c^+ = \Phi_c^- = \Phi_o$) and $\chi = 2\delta$ at $\Phi_c^+ = \Phi_c^- = \pi/2$.

6. Inversion between the inversion and the unwinding lines

In thick samples, with thickness $D > |Z|$, the unwinding lines are situated generally very near to the sample

Downloaded At: 10:03 26 January 2011

surfaces [18–20] leaving the central part of the sample with the helicoidal molecular order. In the sample with a chevron layer deformation, the unwinding lines (i.e. $\pm 2\pi$-twist disclinations) can be observed in the upper and lower part of chevron and the relative position of those lines (they are either superimposed [18] or shifted relatively for $|Z|/2$ [19]) depends on the anchoring conditions on the sample surfaces and on the chevron interfaces. As the chevron interface plays the role of the special supplementary surface in the sample with relatively strong anchoring energy, there will therefore be unwinding lines situated near the chevron interface. If there is an inversion line in this interface, it will interact elastically with the unwinding lines. Suppose now that both the inversion line situated at $x = D_o$, $z = 0$ and the 2π-twist disclination at $x = d$ and $z = z_o$ are oriented along the y axis. The solution of equation (8) describing 2π-twist disclination can be written in a similar form to that in [31]:

$$\Phi_{2\pi} = -S\left\{\arctan\left[\tanh\left(\frac{\pi(z-z_o)}{2\alpha(D-D_o)}\right)\times\operatorname{cotan}\left(\frac{\pi(x-d)}{2(D-D_o)}\right)\right]+\arctan\left[\tanh\left(\frac{\pi(z-z_o)}{2\alpha(D-D_o)}\right)\times\operatorname{cotan}\left(\frac{\pi(x+d-2D)}{2(D-D_o)}\right)\right]\right\}+C, \tag{18}$$

where $S = \pm 1$. The constant C, however, can be different in different parts of the sample depending on the boundary conditions [31]. For the investigation of the interaction between the inversion and unwinding lines, this constant is not important and we put $C = 0$.

The interaction energy between the 2π-twist disclination described by the solution (18) and the inversion line given by (9 *a*), with both lines in the upper part of chevron, can be evaluated as

$$W_1 = \int_{-\infty}^{+\infty} dz\, B_1\left[\Phi_{2\pi}\frac{\partial\Phi^+}{\partial z}\right]_{x=D_o}^{x=D} = \sqrt{(B_1B_3)}(S\Omega^+)\ln\left|\frac{\cosh\dfrac{\pi R}{\alpha(D-D_o)}}{\cosh\dfrac{\pi z_o}{\alpha(D-D_o)}-\cos\dfrac{\pi(d-D_o)}{(D-D_o)}}\right|,$$

with $\Omega^+ = -\Delta\Phi^+$. So there is either a repulsion or an attraction of the unwinding line to the inversion line which depends on the sign of $(S\Omega^+)$ as can be seen from the expression for the x component of the interaction force (per unit length of line):

$$f_x = -\frac{\partial W_1}{\partial d} = \frac{\pi\sqrt{(B_1B_3)}(S\Omega^+)}{D-D_o}\times\frac{\sin\dfrac{\pi(d-D_o)}{D-D_o}}{\cosh\dfrac{\pi z_o}{\alpha(D-D_o)}-\cos\dfrac{\pi(d-D_o)}{(D-D_o)}}. \tag{19}$$

A similar expression can be also written for the case of the unwinding line in the lower part of the chevron.

On the other hand, the unwinding line is repulsed from the sample surfaces when the energy of anchoring is sufficiently high. The expression for this repulsion force was given in [31] and in our notation it can be transformed to the form

$$g_x = \frac{(\pi S)^2\sqrt{(B_1B_3)}}{D-D_o}\operatorname{cotan}\frac{\pi(d-D_o)}{D-D_o}. \tag{20}$$

The equilibrium position can be found for $z_o = 0$ and d satisfying the equation

$$g_x + f_x = 2\pi q B_3, \tag{21}$$

where the term $2\pi q B_3$ is the force due to the helicoidal order in the sample volume which pushes the unwinding line to the sample surface [20, 32].

Supposing that the distance $\Delta d = d - D_o$, which is the distance between the unwinding and inversion lines, is always smaller than the thickness $D - D_o$. Then

$$\Delta d = \frac{|Z|}{4\pi\alpha}(1 + 2kS), \tag{22}$$

where $k = \Omega^+/\pi$. The distance Δd decreases when $S = -1$, i.e. when the inversion line and the unwinding lines attract each other. For $\Phi_o \sim 53°$ and $\alpha \sim 0{\cdot}32$, the value of Δd can be estimated as $\Delta d \sim 0{\cdot}56|Z|/4\pi = 0{\cdot}045|Z|$.

In this estimation, both inversion and unwinding lines are parallel to the y axis. It should be noted that this orientation corresponds to the minimum of their elastic self-energies if $B_3 < B_1$ as can be found using the same procedure shown in [31].

7. Discussion and conclusion

The asymmetric and symmetric inversion lines and their elastic and core energies were discussed in §§ 4 and 5. According to our estimations, the symmetric inversion line has the lower elastic self-energy and core energy because the smectic molecules rotate over the smaller part of the cone (see figure 3).

As for the mechanism of the inversion line creation, a few remarks will be given here. One can imagine that during the phase transition from smectic A to smectic C* with the simultaneous chevron creation, the chevron

Downloaded At: 10:03 26 January 2011

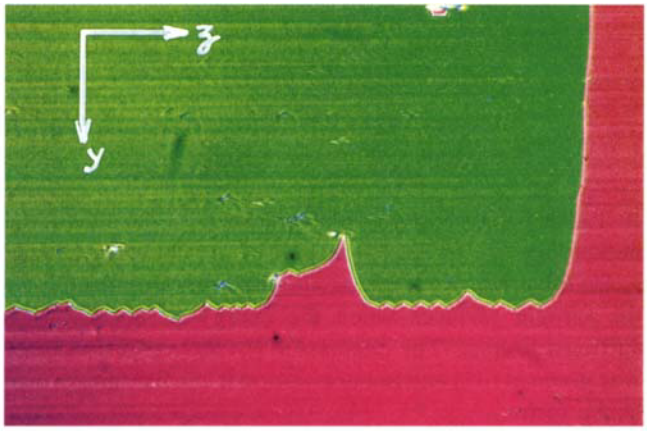

Figure 6.

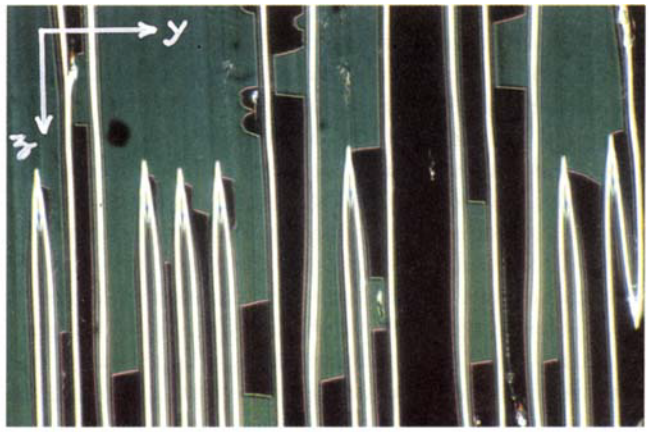

Figure 7.

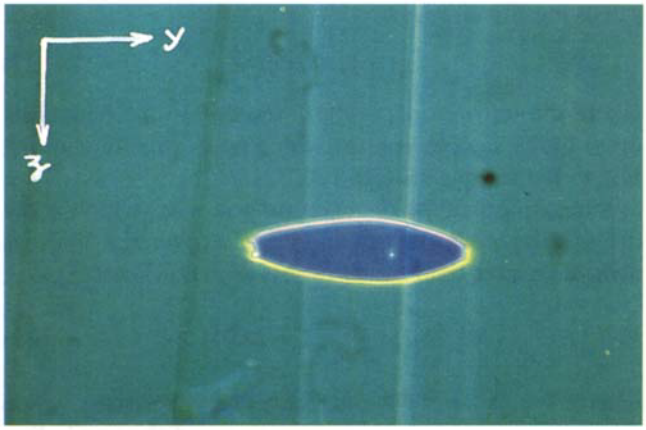

Figure 8 (*a*)

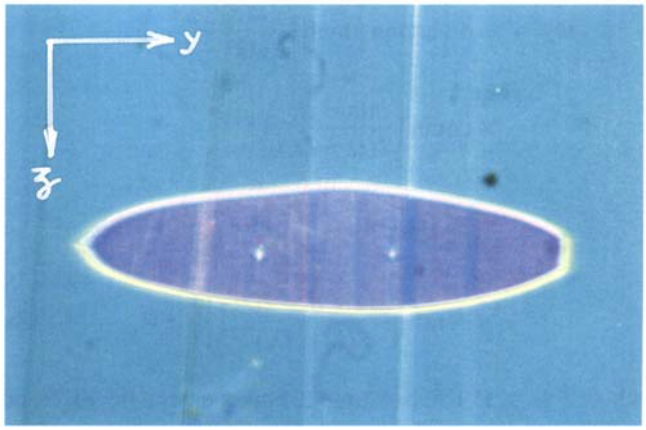

Figure 8 (*b*)

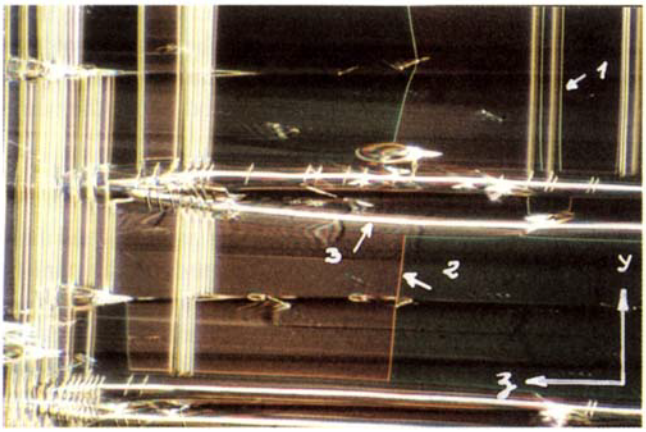

Figure 9.

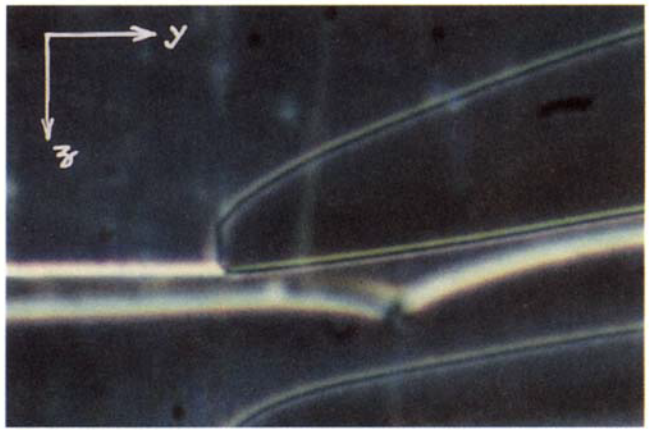

Figure 10.

Downloaded At: 10:03 26 January 2011

interface is not necessarily situated exactly at the distance $D/2$ from the sample surfaces, i.e. the chevron is not symmetric [8]. In thin samples of the thickness smaller than 2 μm, even a small deviation of the chevron position from the sample centre influences the twist deformation which therefore occurs in this part of the sample above or below the chevron interface which is the thicker. When the zigzag defect is present, there could be differences in the positions of the chevron interfaces on both sides of the zigzag [9] and then the zigzag defect coincides with the inversion line. Such a situation was also confirmed by our observations [16, 17] and by the present observation. We observed the textures of cells filled with the compound ZLI 3774 of Merck exhibiting the smectic C* phase between − 30°C and 62°C. The spontaneous pitch at 20°C is − 4 μm.

Figure 6 shows isolated inversion lines where the sample thickness is 6 μm. Colours on both sides of the lines are different because the distribution of the director is not the same [16, 17] and extinction is not possible because the propagation of the light is out of the Mauguin limit. The numerical simulations of the optical contrast of the cell with the chevron interface separating the uniform and twisted arrangements of molecules were reported in [16, 17]. In these simulations, the twist assumed to take part over the smaller segment of the cone and the contrast obtained is coherent with the contrast observed on different sides of an isolated inversion line. These simulations indicate that the observed inversion line is probably the symmetric inversion line.

Figure 7 shows zigzag defects with inversion lines where the sample thickness is 9 μm. Some parts are extinguished with uncrossed polarizers because we are now in the Mauguin domain. Inversion lines still separate one domain where the twist takes place in the upper part of the chevron from another one where the twist is in the lower part.

The glass surfaces with ITO electrodes were coated by SiO. When a small d.c. voltage of about 2 V was applied to the cell, the inversion lines which are present in the sample start to move or new inversion lines are created on the zigzag defects. The movement of inversion lines is the consequence of reorientation of the **t** vector on the upper and lower part of the chevron interface. From the two types of boundary values Φ_c^+ and Φ_c^- shown in figure 2 (*b*), those are preferred which give the molecular spontaneous polarization oriented generally in the electric field direction as discussed in detail in [5, 8, 9]. Because the reorientation starts on the chevron interface, the anchoring energy of the chevron interface γ is smaller compared with the anchoring energies γ_1 of the sample surfaces.

In thicker samples, small deviations of the chevron interface position from the sample centre are not so important, because the twist deformation energies are not so different in this case. Therefore in thicker samples, isolated inversion lines which are not directly associated with zigzag defects can be observed. When again a small electric field with chosen polarity is applied, it leads to the movement of the isolated inversion lines (see figure 8) and annihilation of inversion line loops, leaving the sample with the twist deformation either above or below the chevron interface only.

Nevertheless, the inversion line creation can be associated with irregularities of the interface either of the type of the mountain-like defect or changes in molecular orientation due to the presence of defects in the chevron interface, for example, the 2π-disclination shown in figure 5 (*a*) or perhaps some point defects (two white dots seen inside the inversion line loop in figure 8). The presence of those defects in the chevron interface can assist the change of the **t** vector orientations on the chevron interface characterized by the boundary values Φ_c^+ and Φ_c^-. When changing the electric field polarity, it is clearly seen that inversion lines are created on other defects in the sample.

The observation of systems of unwinding lines together with inversion lines [33] shows the following features:

(i) When the inversion line occurs, it changes, for example, symmetric anchoring conditions to parallel anchoring conditions in the upper part of chevron and

Figure 6. Inversion line separates two domains (chevron surface domains [5, 9]) of different colours. This and the subsequent photographs show the inversion lines in samples of the liquid crystal ZLI 3774 in the FLC phase. The spontaneous pitch is − 4 μm, and the cell thickness 6 μm.

Figure 7. Zigzag defect and inversion lines. Parts of inversion lines are attached to segments of the zigzag defect. Other parts of inversion lines of the area limited by zigzag defect thereby separating the different molecular orientations in the chevron interface (chevron surface domains), see also [3, 5, 8, 9, 15, 16]. In this case the extinction of some domains is obtained with uncrossed polarizers due to the twisted state in a cell which is in the Mauguin domain for the propagation of light (9 μm).

Figure 8. The increase of the area limited by the inversion line loop under the influence of an applied electric field (sequence of (*a*) to (*b*)). This inversion line loop was created on some other defects in the chevron interface.

Figure 9. Unwinding and inversion lines in the area where the thickness of the cell (15 μm) is of the order that permits the helicoidal structure. Here inversion lines also separate two domains where the twist is not located on the same side of the chevron, either going with the unwinding lines (1) or in the unwound part (2). The long segments of both types of line are oriented along the smectic layers. Zigzag defects (3) perpendicular to the lines are also present.

Figure 10. Unwinding and inversion lines. In this photograph, parts of the unwinding lines coincide with the inversion line due to their mutual attraction. The overlapping parts of lines have different optical contrasts.

Downloaded At: 10:03 26 January 2011

vice versa in the lower part of the chevron. When the sample thickness is such that it permits the existence of unwinding line pairs which are relatively shifted for $|Z|/2$ [20, 34], the unwinding lines exist only in the parts of the sample between the surfaces and the chevron interface with symmetric anchoring conditions. In the parts of the sample with parallel anchoring conditions, no unwinding lines exist. As discussed in [20, 34] parallel anchoring conditions favour superimposed unwinding lines which are stable for greater sample thickness when compared with sample thickness permitting the occurrence of shifted unwinding lines. Nevertheless, in samples with shifted lines, different situations can be observed. In this contribution two cases will be mentioned. In the first case the shifted unwinding lines are either above or below the chevron interface only. Then the inversion line separates the domain, with unwinding lines from the domain without any lines (see figure 9). In the second case, the sample thickness permits the existence of shifted unwinding lines both above and below the chevron interface and their occurrence is determined by the realization of the symmetric anchoring conditions. In this case the inversion line separates the domain with unwinding lines above the chevron interface from the domain where unwinding lines are below the chevron interface. These observations seem to confirm our idea of the inversion line as a boundary between symmetric and parallel anchoring conditions.

(ii) Sometimes the observation of lines reveals that the parts of the inversion and unwinding lines coincide (see figure 10); this can be interpreted as the attraction between both lines given by equation (21). This attraction encourages the unwinding line to occupy the position just above the inversion line at the distance which can be estimated by (22).

(iii) The observations also show that the long segments of both unwinding and inversion lines are oriented along the smectic layers (in our coordinate system the orientation of these long segments coincides with the y-axis). This can be a consequence of the anisotropy of the elastic constants B_1 and B_3 which leads to the relation $B_3 < B_1$.

In conclusion, the results of this contribution can be listed as follows:

(1) The simplified model of the inversion line in FLC with the chevron layer structure was proposed using the simplified smectic C* elasticity. Our model is based on the assumption that the chevron interface acts as a supplementary interface in the FLC sample which plays the role of the energetic barrier preventing the propagation of the **t** vector twist deformation into the whole sample. The inversion line is represented by a pair of surface twist disclinations situated on the upper and lower chevron interfaces, respectively. Those surface disclinations are related by the chevron interface energy (4).

Our model does not take into account the influence of the spontaneous polarization P_s on the **t** vector distribution near the inversion line and therefore it is restricted to the FLC materials with the small values of P_s.

(2) Two possible solutions called the asymmetric and symmetric inversion lines are proposed. The energy considerations reached within our approximation show that the symmetric inversion line would be favourable.

(3) When $\gamma_1 > \gamma$, the application of a small electric field to the sample reorients first the **t** vector orientation on the chevron interface in agreement with the observations and conclusions in [5, 8, 9]. The **t** vector reorientation leads either to the movement of the existing inversion line or to the creation of inversion line loops on other defects in the sample.

(4) In the case that the interaction of the inversion line with the unwinding line is attractive, the segments of both lines are situated very near to each other so that their optical contrasts can coincide.

The authors would like to express their thanks to Dr Laurent Limat for discussions of the chevron profile in chiral smectic C* liquid crystals and for communicating his results prior to their publication.

One of the authors (L.L.) would like to acknowledge the financial support of the French Ministère de la Recherche et de l'Espace during his stay at the Université de Montpellier. He also benefited by the grant AVCR No. 19062 and by the grant No. 202/93/1155 of the Grant Agency of the Czech Republic.

References

[1] Handschy, M. A., and Clark, N. A., 1984, *Ferroelectrics*, **59**, 69.
[2] Rieker, T. P., Clark, N. A., Smith, G. S., Parmer, D. S., Sirota, E. B., and Safinya, C. R., 1987, *Phys. Rev. Lett.*, **59**, 2658.
[3] Ouchi, Y., Takano, H., Takezoe, H., and Fukuda, A., 1988, *Jap. J. appl. Phys*, **27**, 1.
[4] Hiji, N., Ouchi, Y., Takezoe, H., and Fukuda, A., 1988, *Jap. J. appl. Phys.*, **27**, L1.
[5] Clark, N. A., Rieker, T. P., and Maclennan, J. E., 1988, *Ferroelectrics*, **85**, 79.
[6] Clark, N. A., and Rieker, T. P., 1988, *Phys. Rev.* A, **37**, 1053.
[7] Fukuda, A., Ouchi, Y., Arai, H., Takano, H., Ishikawa, K., and Takezoe, H., 1989, *Liq. Crystals*, **5**, 1055.
[8] Maclennan, J. E., Clark, N. A., Handschy, M. A., and Meadows, M. R., 1990, *Liq. Crystals*, **7**, 753.
[9] Maclennan, J. E., Handschy, M. A., and Clark, N. A., 1990, *Liq. Crystals*, **7**, 787.
[10] Willis, P. C., Clark, N. A., and Safinya, C. R., 1992, *Liq. Crystals*, **11**, 581.
[11] Willis, P. C., Clark, N. A., Xue, J.-Z., and Safinya, C. R., 1992, *Liq. Crystals*, **12**, 891.
[12] Sato, Y., Tanaka, T., Nagata, M., Takeshita, H., and Morozumi, S., 1987, *Proc. SID*, **28**, 189.
[13] Zhuang, Z., Rappaport, A. G., and Clark, N. A., 1993, *Liq. Crystals*, **15**, 417.

Downloaded At: 10:03 26 January 2011

[14] ELSTON, S. J., and SAMBLES, J. R., 1990, *Jap. J. appl. Phys.*, **29,** L641.
[15] BRUNET, M., 1993, *Program Book of Abstracts* (4th International Conference on Ferroelectric Liquid Crystals, Tokyo), p. 187.
[16] QUENTEL, S., 1993, Thèse, Université de Montpellier II.
[17] QUENTEL, S., and BRUNET, M., 1993, *Ferrolelectrics*, **149,** 139.
[18] BRUNET, M., and WILLIAMS, C., 1978, *Ann. Physique*, **3,** 237.
[19] GLOGAROVÁ, M., and PAVEL, M., 1984, *J. Physique (France)*, **45,** 143.
[20] BRUNET, M., and MARTINOT-LAGARDE, PH., 1994, *J. Physique II (France)*, to be published.
[21] KLÉMAN, M., 1983, *Points, Lines, and Walls in Liquid Crystals, Magnetic Systems and Various Ordered Media* (Wiley, New York).
[22] NAKAGAWA, N., 1989, *Molec. Crystals liq. Crystals*, **174,** 65.
[23] NAKAGAWA, N., 1990, *J. Phys. Soc. Japan*, **59,** 1995.
[24] LIMAT, L., and PROST, J., 1993, *Liq. Crystals*, **13,** 101.
[25] MUKAI, S., and NAKAGAWA, M., 1993, *J. Phys. Soc. Japan*, **62,** 1984.
[26] DE MEYERE, A., PAUWELS, H., and DE LEY, E., 1993, *Liq. Crystals*, **14,** 1269.
[27] LIMAT, L., *J. Physique II (France)*, to be published.
[28] BOURDON, L., SOMMERIA, F., and KLÉMAN, M., 1982, *J. Physique (France)*, **43,** 77.
[29] LEJČEK, L., MARCEROU, J. P., DESTRADE, C., and DUPONT, L., 1989, *J. Physique (France)*, **50,** 361.
[30] VÍTEK, V., and KLÉMAN, M., 1975, *J. Physique (France)*, **36,** 59.
[31] LEJČEK, L., GLOGAROVÁ, M., and PAVEL, J., 1984, *Phys. stat. Sol. (a)* **82,** 47.
[32] GLOGAROVÁ, M., LEJČEK, L., PAVEL, J., LANOVEC, V., and FOUSEK, J., 1983, *Molec. Crystals liq. Crystals*, **91,** 309.
[33] BRUNET, M., to be published.
[34] LEJČEK, L., 1985, *Czech. J. Phys.* B, **35,** 655.

Downloaded At: 10:03 26 January 2011